Power Electronic Systems
Laboratory



Proceedings of the 27th Applied Power Electronics Conference and Exposition (APEC 2012), Orlando Florida, USA,
February 5-9, 2012

# Design of a Minimum Weight Dual Active Bridge Converter for an Airborne Wind Turbine System

R. A. Friedemann,
F. Krismer,
J. W. Kolar



Eidgenössische Technische Hochschule Zürich
Swiss Federal Institute of Technology Zurich

# Design of a Minimum Weight Dual Active Bridge Converter for an Airborne Wind Turbine System

R. A. Friedemann, F. Krismer, and Johann W. Kolar
Power Electronic Systems Laboratory
ETH Zürich
Zürich, Switzerland
Email: friedemann@lem.ee.ethz.ch

***Abstract*— The design procedure for a bidirectional DAB dc–dc converter, which provides a high dc voltage of 8 kV to the tether of a 100 kW Airborne Wind Turbine (AWT) system, is presented. The maximum allowed weight of the dc–dc converter is 25 kg and, thus, the main challenge is the realization of a light-weight DAB converter. The investigated dc–dc converter is split up into 16 single DAB modules with a rated power of 6.25 kW and a dc port voltage of 2 kV. Thus, a weight of less than $25\,\mathrm{kg}/16 = 1.56\,\mathrm{kg}$ needs to be achieved for a single DAB module. The design method used to obtain the minimum weight DAB converter, based on the evaluation of a power-to-weight ratio versus efficiency Pareto Front ($\gamma$-$\eta$-Pareto Front) is presented in this paper. For this purpose the transient voltages and currents of the employed SiC JFETs during switching are discussed in detail, since the respective measurement results allow for a prediction of the switching losses. Moreover, the calculated transformer is realized and experimental results are used to verify the weight, the losses, and the cooling system performance of the transformer. For a single DAB module a weight of $m = 1.43\,\mathrm{kg}$, an efficiency of $\eta = 97\%$, and a power-to-weight ratio of $\gamma = 4.4\,\mathrm{kW/kg}$ results.**

## I. Introduction

Recent research on wind power generation proposes the use of airborne wind turbines (AWT) [1]–[4] that take advantage of high-altitude winds, which are faster and more consistent than the winds near to the Earth's surface [2]. The AWT needs to be lightweight [5] and, thus, the different parts of the AWT are optimized with respect to low weight.

Fig. 1 depicts the electrical system of the AWT presented in [5]. It is composed of 8 motors / generators (motor operation is needed to start-up the system), 8 inverters / rectifiers, 4 isolated and bidirectional dc–dc converters, the tether (provides the mechanical and the electrical connection between the AWT and the ground station), and the ground station. The specified rated power of the investigated system is 100 kW for generator and motor operation; between the airframe of the kite and the tether a galvanic isolation is required.

The realization of the bidirectional and light-weight dc–dc converters is one of the main challenges in the design of the AWT system and is the central element of this paper. The required specifications of a single dc–dc converter are listed below.

- Rated output power: $P_{\mathrm{out}} = 100\,\mathrm{kW}/4 = 25\,\mathrm{kW}$
- Low Voltage (LV) port: $650\,\mathrm{V} \leq V_1 \leq 750\,\mathrm{V}$

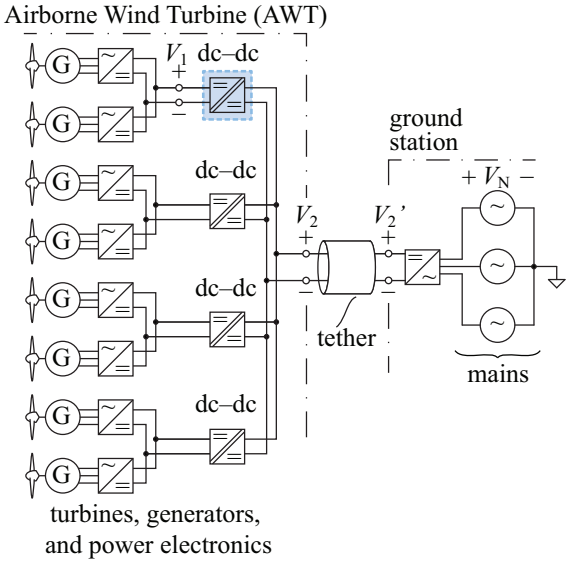


Fig. 1. AWT basic electric structure [5]; here, the focus is on the highlighted dc–dc converter (rated power: 25 kW), which is shown in Fig. 2.

- Medium Voltage (MV) port: $V_2/V_1 = 8\,\mathrm{kV}/750\,\mathrm{V}$, i.e. $V_2/V_1$ = const., $6.9\,\mathrm{kV} \leq V_2 \leq 8\,\mathrm{kV}$
- Maximum weight: $m_{\mathrm{max}} = 6.25\,\mathrm{kg}$.

Based on these requirements the modified DAB converter topology [6], depicted in Fig. 2(a), is considered to be most suitable. Its soft switching capability enables high switching frequency operation, the power transfer characteristic is independent of the direction of power flow, and it requires a low number of heavy magnetic components. The 3-level Neutral Point Clamped (NPC) converter on the MV side reduces the maximum blocking voltages applied to $\mathrm{T}_5 \ldots \mathrm{T}_8$ to $1/2$ of the port voltage $V_{2,i}$ and also reduces the maximum transformer voltage to $|v_{\mathrm{ac2}}| \leq V_{2,i}/2$, which is advantageous regarding the isolation requirements of the MV side transformer winding.

A high switching frequency is employed in order to achieve a low weight of the high frequency (HF) transformer and the inductor. The switching frequency used, $f_{\mathrm{S}} = 100\,\mathrm{kHz}$, is selected based on previous design results and yields a

978-1-4577-1216-6/12/$26.00 ©2012 IEEE

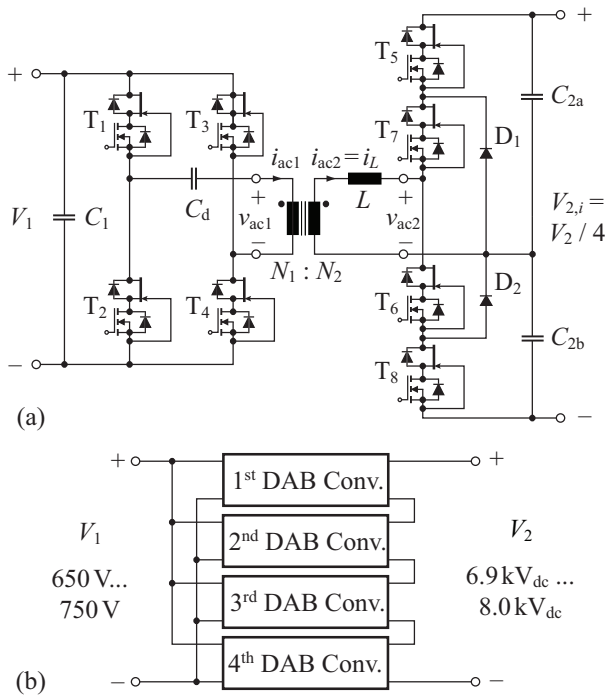


Fig. 2. (a) Single modified DAB converter [6] (rated power: 6.25 kW); (b) proposed interconnection of 4 DAB converters to achieve a rated power of 25 kW and $V_2 \leq 8\,\mathrm{kV}$.

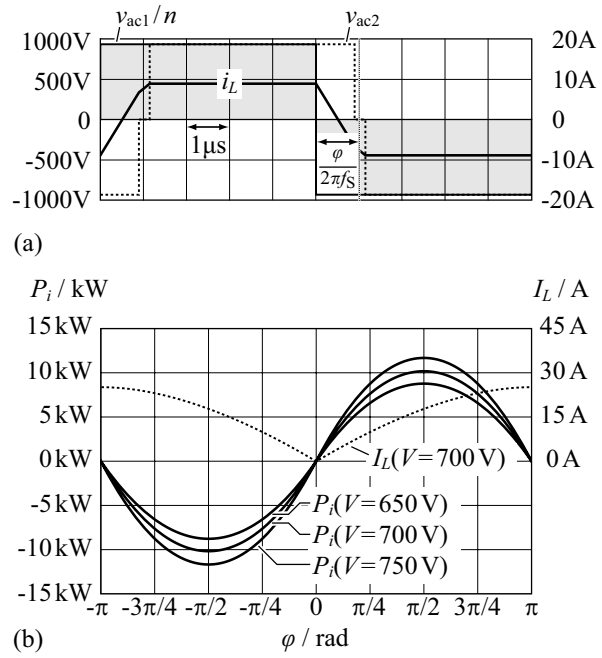


Fig. 3. (a) Calculated voltage and current waveforms for a single DAB converter ($V_1 = 700\,\mathrm{V}$, $V_{2,i} = 1.9\,\mathrm{kV}$, $P_i = 6.25\,\mathrm{kW}/\eta_{\mathrm{exp}}$, $\eta_{\mathrm{exp}} = 95\%$, $n = 0.75$, $L = 107\,\mu\mathrm{H}$, $f_{\mathrm{S}} = 100\,\mathrm{kHz}$); the NPC converter on the MV side requires a freewheeling time of 250 ns in order to ensure equal blocking voltages of the series connected switches. (b) Power transfer characteristics of the DAB (calculated according to [8]), $V_1/V_{2,i} = 0.75 =$ constant; maximum power transfer is achieved for $\varphi = \pm\pi/2$; the dashed line depicts the rms inductor current $I_L(\varphi)$ at nominal operation.

reasonable compromise between converter losses and weight.[1]

The DAB converter to be designed employs SiC JFET switches ($R_{\mathrm{DS,on}} = 150\,\mathrm{m\Omega}$ at $T_{\mathrm{j}} = 150°\mathrm{C}$, normally-on, max. blocking voltage: 1700 V) in cascode connection with LV MOSFETs which facilitate a high switching frequency and normally-off characteristic [7]. The series connection of 4 converters, depicted in Fig. 2(b), is used to obtain a maximum blocking voltage of 1000 V for $\mathrm{T}_5 \ldots \mathrm{T}_8$. The rated output power of a single DAB converter is $P_{2,i} = 6.25\,\mathrm{kW}$.

This paper summarizes the basic design of a minimum weight DAB converter in **Section II**. **Section III** presents the calculation of the converter losses, since the final converter design is based on the evaluation of a power-to-weight ratio versus efficiency Pareto Front ($\gamma$-$\eta$-Pareto Front). **Section IV** discusses the weight optimized design of the HF transformer, the inductor, and all required heat sinks. Furthermore, the resulting $\gamma$-$\eta$-Pareto Front is presented in Section IV.

## II. DAB Converter Design

The employed DAB converter is operated most efficiently at $V_1 \approx V_{2,i}/2$ [8]. Thus, $n$ is calculated according to:

$$n = \frac{V_1}{V_{2,i}/2} = \frac{750\,\mathrm{V}}{1\,\mathrm{kV}} = 0.75. \tag{1}$$

There, the conventional modulation scheme (cf. [9]) yields minimum converter losses and low switching losses [8].

[1]Different weight optimal converters have been calculated for $f_{\mathrm{S}} = 50\,\mathrm{kHz}$, 80 kHz, 100 kHz, 125 kHz, 160 kHz, and 200 kHz.

However, the MV side NPC converter requires a minimum freewheeling time of 250 ns in order to ensure equal blocking voltages of the series connected switches and, thus, slightly modified voltage and current waveforms result [Fig. 3(a)]. The minimum inductance needed to achieve a certain rated power of the DAB converter can be calculated with:

$$L = \frac{\min(V_1 V_{2,i})}{4 n f_{\mathrm{S}} \frac{P_{i,\max}}{\eta_{\mathrm{exp}}}} \left[ -\frac{\varphi_{\max}^2}{\pi^2} + \frac{\varphi_{\max}}{\pi} - \left( \frac{1}{2} - D_2 \right)^2 \right] = 107\,\mu\mathrm{H} \tag{2}$$

($P_{i,\max} = 6.25\,\mathrm{kW}$, $\eta_{\mathrm{exp}} = 95\%$, $f_{\mathrm{S}} = 100\,\mathrm{kHz}$, $D_2 = 5\,\mu\mathrm{s} - 250\,\mathrm{ns})/10\,\mu\mathrm{s} = 0.475$). The maximum phase angle is selected in order to achieve low conduction losses at rated output power (small $\varphi_{\max}$ is preferable) and good controllability at low power levels [large $\varphi_{\max}$, i.e. $\varphi_{\max} = \pi/2$, is preferable; cf. Fig. 3(b)]. Typical values for $\varphi_{\max}$ are in the range between $\pi/4$ and $\pi/3$; the presented DAB converter is designed for $\varphi_{\max} = \pi/4$ [5]. Tab. I lists the calculated transformer and capacitor currents.

## III. DAB Converter Losses

The estimation of the $\gamma$-$\eta$-Pareto Front requires the losses and the weights of all components of the DAB converter to be known, which is detailed in this Section and in the subsequent Section IV.

TABLE I

TRANSFORMER AND CAPACITOR CURRENTS OF A SINGLE DAB CONVERTER MODULE WITH $P_i = 6.25\,\mathrm{kW}/\eta_{\mathrm{EXP}}$ AND $\eta_{\mathrm{EXP}} = 95\%$.

| Property | Value | Description |
|---|---|---|
| $\max(I_{\mathrm{ac1}})$ | 12.2 A | Max. rms transformer current, LV side |
| $\max(I_{\mathrm{ac2}})$ | 9.2 A | Max. rms transformer current, MV side |
| $\max(I_{\mathrm{ac2,peak}})$ | 10.2 A | Max. peak inductor current |
| $\max(I_{\mathrm{C1}})$ | 7.0 A | Max. rms capacitor current of $C_1$ |
| $\max(I_{\mathrm{C2}})$ | 5.3 A | Max. rms capacitor current of $C_{2\mathrm{a}}$ and $C_{2\mathrm{b}}$ |

TABLE II

PARAMETERS USED TO CALCULATE THE CONDUCTION LOSSES.

| $R_{\mathrm{DS,on}}$ at $T_{\mathrm{j}} = 25°\mathrm{C}$ | $R_{\mathrm{DS,on}}$ at $T_{\mathrm{j}} = 150°\mathrm{C}$ | Description |
|---|---|---|
| 80 mΩ | 150 mΩ | On-state resistance of the JFET |
| $R_{\mathrm{DS,on}}$ at $T_{\mathrm{j}} = 25°\mathrm{C}$ | $R_{\mathrm{DS,on}}$ at $T_{\mathrm{j}} = 125°\mathrm{C}$ | |
| 5.5 mΩ | 8.3 mΩ | On-state resistance of the MOSFET |

The considered losses are the semiconductor's conduction and switching losses and the copper and core losses of the inductor and the HF transformer.

### A. Conduction Losses

The conduction losses are determined using the RMS switch currents, which are calculated according to [10], and the on-state resistances of the SiC JFETs, $R_{\mathrm{DS,on,JFET}} = 150\,\mathrm{m\Omega}$ ($T_{\mathrm{j}} = 150°\mathrm{C}$), and the MOSFET (IRF4104S), $R_{\mathrm{DS,on,MOSFET}} = 8.3\,\mathrm{m\Omega}$ ($T_{\mathrm{j}} = 125°\mathrm{C}$) [10].

### B. Switching Losses

The switching losses of the full bridge and the NPC converter are calculated based on measurement values, according to [10]. For this purpose, the switching losses of the NPC converter are measured, since the transient processes are – compared to the full bridge – more complex, there. The obtained results facilitate the estimation of the switching losses generated by the full bridge, as described at the end of this section.

The employed measurement method acquires the instantaneous voltages and currents of all 6 power semiconductors of the NPC converter, according to Fig. 4(a), in order to determine the overall energy dissipated in a single switching operation.[2] The pulse signal depicted in Fig. 4(b) reproduces different switching conditions: low switching losses are generated during $t_{1\mathrm{a}} < t < t_{1\mathrm{d}}$ (almost Zero Voltage Switching, ZVS) and increased switching losses, particularly due to reverse recovery effects, can be generated during $t_{2\mathrm{a}} < t < t_{2\mathrm{d}}$ (hard switching). Due to the low switching losses the switching operations during $t_{1\mathrm{a}} < t < t_{1\mathrm{d}}$ are of main interest; Fig. 5 illustrates the respective transient processes with the particular current conduction paths being highlighted in red.

[2]This method is detailed in [11] and yields the switching losses of a single switching operation of a DAB converter operated in steady state.

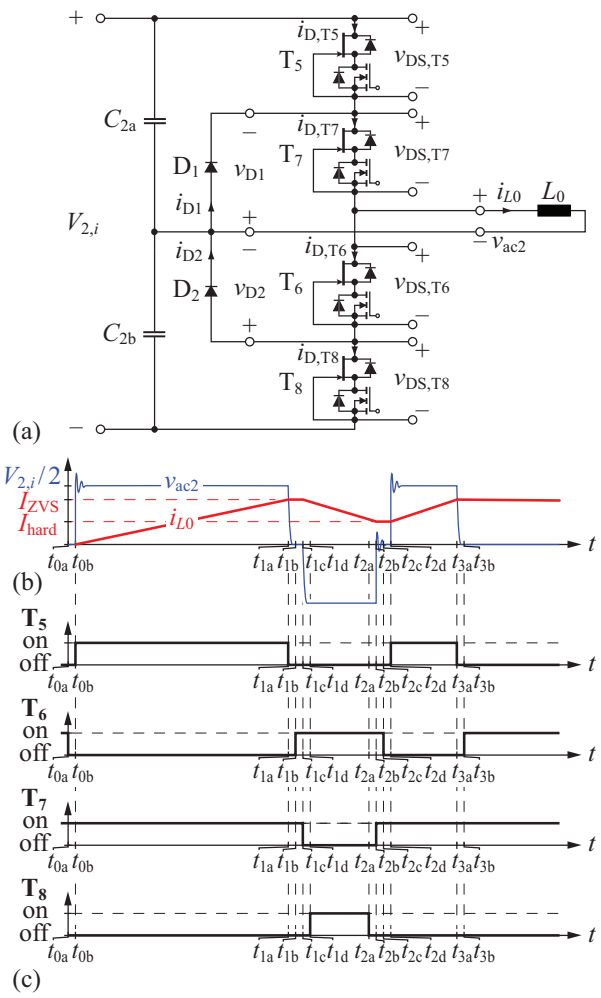


Fig. 4. (a) Switching loss measurement setup (NPC converter); (b) employed measurement waveforms: (almost) ZVS during $t_{1\mathrm{a}} < t < t_{1\mathrm{d}}$, hard switching during $t_{2\mathrm{a}} < t < t_{2\mathrm{d}}$; (c) respective gate signals of $\mathrm{T}_5$, $\mathrm{T}_6$, $\mathrm{T}_7$, and $\mathrm{T}_8$. The dead time used to avoid a shoot through is 200 ns.

These processes, however, are different for $t_{1\mathrm{a}} < t < t_{1\mathrm{b}}$ and $t_{1\mathrm{c}} < t < t_{1\mathrm{d}}$ and are thus discussed separately. The dead time used to avoid a shoot through is 200 ns.

*a) Switching $v_{\mathrm{ac2}}$ from $V_{2,i}/2$ to 0 ($t_{1\mathrm{a}} < t < t_{1\mathrm{b}}$, Fig. 7):* $\mathrm{T}_5$ is turned off at $t = t_{1\mathrm{a}}$ and during $t_{1\mathrm{a}} < t < t'_{1\mathrm{a}}$ the effective output capacitances of $\mathrm{T}_5$, $\mathrm{T}_6$, $\mathrm{T}_8$, $\mathrm{D}_1$, and $\mathrm{D}_2$ ($C_{\mathrm{T5}}$, $C_{\mathrm{T6}}$, $C_{\mathrm{T8}}$, $C_{\mathrm{D1}}$, and $C_{\mathrm{D2}}$, respectively) are either charged or discharged [Fig. 5(b)]. During this time the equivalent circuit shown in Fig. 6(a) can be used to analyze the different charging or discharging processes. At $t = t'_{1\mathrm{a}}$ the diode $\mathrm{D}_1$ starts to conduct and the voltage applied to $C_{\mathrm{T5}}$ is $V_{2,i}/2$. However, the voltage divider formed by $C_{\mathrm{T8}}||C_{\mathrm{D2}}$ and $C_{\mathrm{T6}}$ [Fig. 6(a)] prevents $C_{\mathrm{T6}}$ to be fully discharged, cf. Fig. 7(c) at $t = t'_{1\mathrm{a}}$. $\mathrm{T}_7$ and $\mathrm{D}_1$ conduct the freewheeling current during $t'_{1\mathrm{a}} < t < t_{1\mathrm{b}}$ [Fig. 5(c)] and thus, the switch and diode voltages remain constant during that time interval. At $t = t_{1\mathrm{b}}$

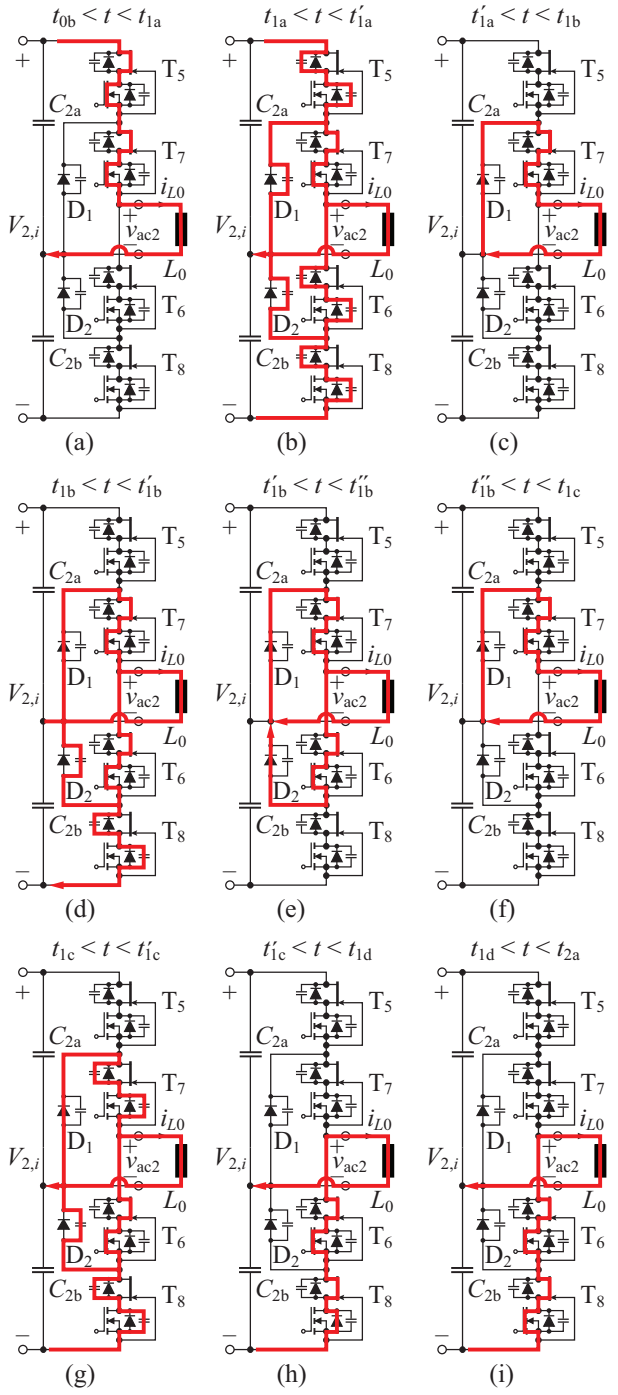


Fig. 5. Transient conduction paths during $t_{1a} < t < t_{1d}$, cf. Fig. 4(b); (a) ... (f): $v_{ac2}$ is switched from $V_{2,i}/2$ to 0; (g) ... (i): $v_{ac2}$ is switched from 0 to $-V_{2,i}/2$.

the switch $T_6$ is turned on [Fig. 5(d)], causing turn-on losses.[3]

[3]The employed method cannot directly determine the remaining energy stored in $C_{T6}$ that is dissipated during $t_{1b} < t < t'_{1b}$. However, the energy required to fully charge $C_{T5}$ during $t_{t1a} < t < t'_{1a}$ is considerably larger than the energy released by $C_{T6}$ during the same time interval. Thus, assuming that $C_{T5}$ and $C_{T6}$ store the same energies at the same blocking voltages, the measurement implicitly includes the remaining energy stored in $C_{T6}$.

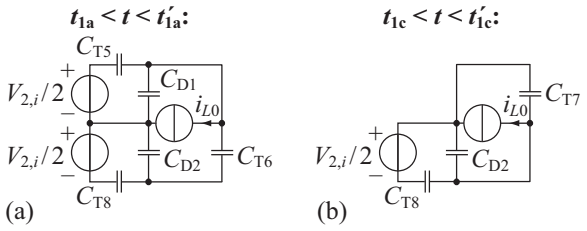


Fig. 6. (a) Simplified equivalent circuit of the NPC converter during $t_{1a} < t < t'_{1a}$; (b) simplified equivalent circuit during $t_{1c} < t < t'_{1c}$.

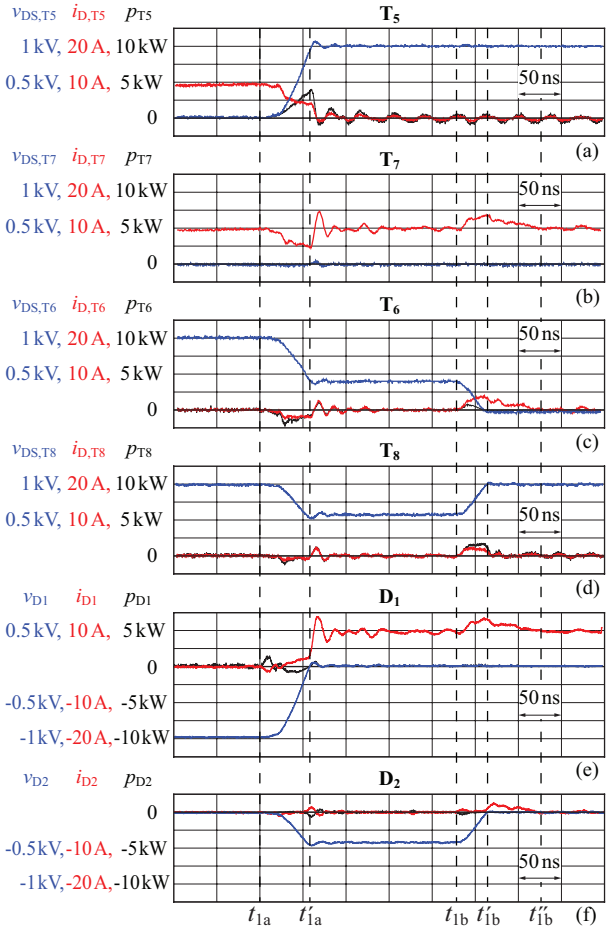


Fig. 7. Measured instantaneous currents and voltages of the switches and diodes of the NPC converter depicted in Fig. 4(a) for $v_{ac2}$ being switched from $V_{2,i}/2$ to 0; $V_{2,i} = 2\,\text{kV}$, $i_{L0}(t_{1a}) = I_{ZVS} = 10\,\text{A}$. During $t_{1b} < t < t'_{1b}$ the switch $T_6$ generates turn-on losses since its effective output capacitance has not been completely discharged during $t_{1a} < t < t'_{1a}$.

$C_{T8}$ is charged to $V_{2,i}/2$ at $t = t'_{1b}$ and, subsequently, $D_2$ starts to conduct the excess current generated during $t_{1b} < t < t'_{1b}$ [Fig. 5(e), current path: $D_2$ – $D_1$ – $T_7$ – $T_6$]. This excess current reduces to zero at $t = t''_{1b}$ [Fig. 5(f)].

*b) Switching $v_{ac2}$ from 0 to $-V_{2,i}/2$ ($t_{1c} < t < t_{1d}$, Fig. 8):* At $t = t_{1c}$ the switch $T_7$ is turned off, which causes $C_{T7}$ and $C_{D2}$ to be charged and $C_{T8}$ to be discharged during $t_{1c} < t < t'_{1c}$ [Fig. 5(g), Fig. 6(b)]. During this time interval a

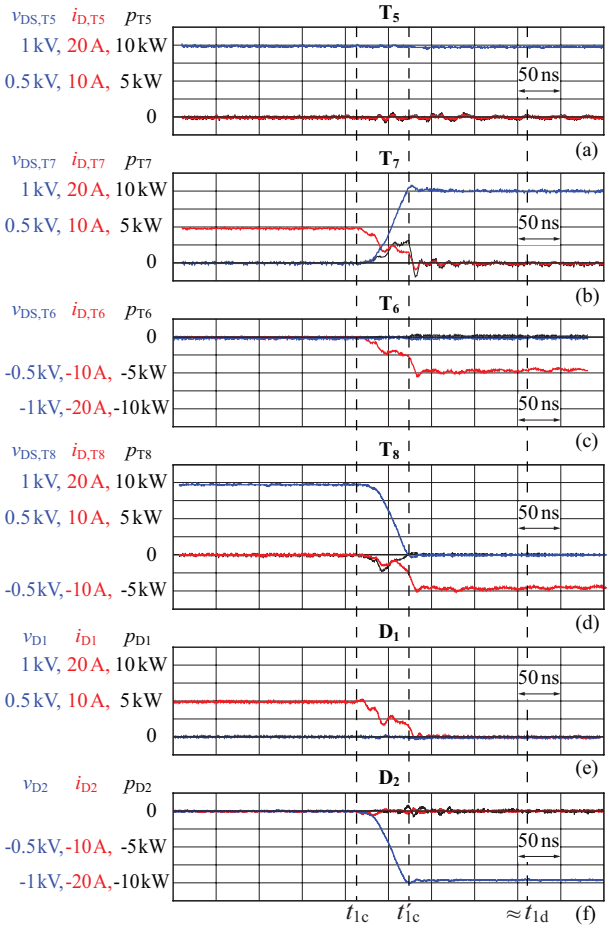


Fig. 8. Measured instantaneous currents and voltages of the switches and diodes of the NPC converter depicted in Fig. 4(a) for $v_{ac2}$ being switched from 0 to $-V_{2,i}/2$; $V_{2,i} = 2\,\text{kV}$, $i_{L0}(t_{1c}) = I_{ZVS} = 10\,\text{A}$. During $t_{1c} < t < t'_{1c}$ the energy stored in the output capacitance of $T_8$ is transferred to that of $T_7$.

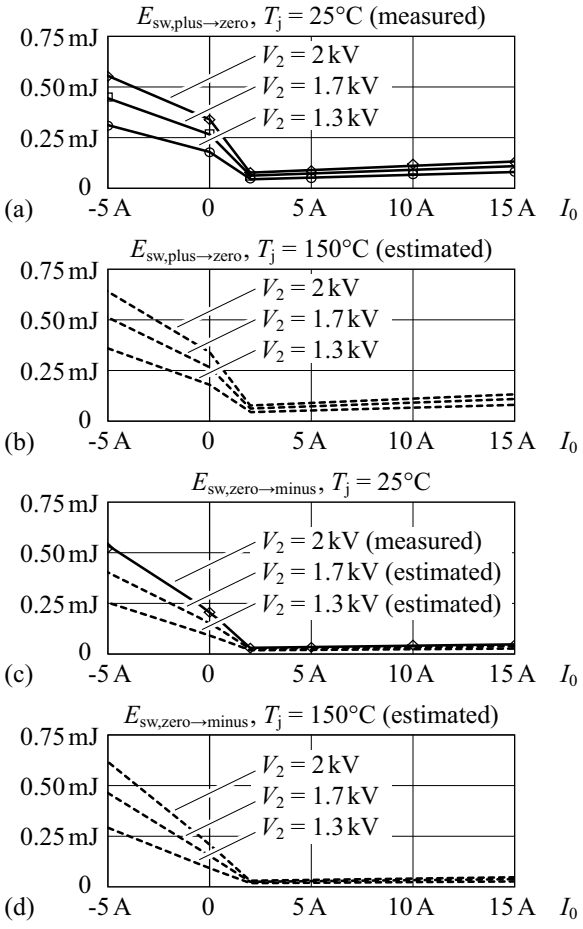


Fig. 9. Switching loss energy dissipated in the NPC converter (Fig. 4) in a single switching operation; (a) and (b) $v_{ac2}$ is switched from $V_{2,i}/2$ to 0; (c) and (d) $v_{ac2}$ is switched from 0 to $-V_{2,i}/2$. A minimum current of 2 A is required to fully discharge the effective output capacitance of the switch which is turned on during the dead time interval of 200 ns. Thus, for $I_0 < 2\,\text{A}$, increasing turn-on losses result for decreasing $I_0$ [8].

considerable amount of the energy stored in $C_{T8}$ is transferred into $C_{T7}$ and $C_{D2}$ (Fig. 8). $C_{T8}$ is fully discharged at $t = t'_{1c}$ and the body diode of $T_8$ conducts $i_{L0}$ during $t'_{1c} < t < t_{1d}$ [Fig. 5(h)]. Finally, $T_8$ is turned on at $t = t_{1d}$ with zero turn-on losses [Fig. 5(i)].

*c) Resulting Switching Losses:* Fig. 9 summarizes the switching losses measured for the two different switching operations, i.e. Fig. 9(a) shows the switching losses obtained for switching $v_{ac2}$ from $V_{2,i}/2$ to 0 and Fig. 9(c) shows the switching losses obtained for switching $v_{ac2}$ from 0 to $-V_{2,i}/2$. Positive currents $I_0 > 2\,\text{A}$ denote the ZVS range where low switching loss energies in the range between 20 µJ and 150 µJ result. For $I_0 < 0$ turn-on losses due to reverse recovery cause the switching losses to increase. For $0 < I_0 < 2\,\text{A}$ the duration of the dead time interval of 200 ns is insufficient to allow for a full discharge of the switch which is turned on. Thus, in this range, increasing turn-on losses result for decreasing $I_0$ [11].

The switching loss measurement has been carried out at room temperature. The switching losses which are expected at an elevated junction temperature of the SiC JFET of $T_j = 150°\text{C}$ are estimated based on previous switching losses measured at $T_j = 150°\text{C}$ for the same SiC JFET: according to these measurements only a negligible change results for ZVS and at $I_0 = -5\,\text{A}$ the turn-on losses due to reverse recovery increase by $\approx 15\%$. The switching losses depicted in Fig. 9(c) for $V_{2,i} = 1.3\,\text{kV}$ and $V_{2,i} = 1.7\,\text{kV}$ are estimated based on the previous results.

Equal switching losses are expected if $v_{ac2}$ is switched from $-V_{2,i}/2$ to $V_{2,i}/2$, i.e.

$$E_{sw,plus\rightarrow zero} = E_{sw,minus\rightarrow zero}, \quad (3)$$

$$E_{sw,zero\rightarrow minus} = E_{sw,zero\rightarrow plus}. \quad (4)$$

Moreover, switch currents and voltages similar to those of Figs. 8 (b) and (d) are expected for the LV side full bridge and therefore, the respective switching losses [$E_{sw,zero\rightarrow minus}$, Figs. 9 (c) and (d)] are used to estimate the switching losses of the full bridge, too.

### C. Copper and Core Losses

The copper losses are calculated based on the RMS value of $i_L$ and the copper resistances of the HF transformer and inductor windings [10]. The Steinmetz equation is used to determine the core losses:

$$P_{\text{tr,core}} = V_{\text{tr,core}} k f_S^{\alpha} B_{\text{tr,peak}}^{\beta} \text{ and } P_{\text{ind,core}} = V_{\text{ind,core}} k f_S^{\alpha} B_{\text{ind,peak}}^{\beta} \tag{5}$$

[$V_{\text{tr,core}}$ and $V_{\text{ind,core}}$ denote the core volumes of the transformer and the inductor; $B_{\text{tr,peak}}$ and $B_{\text{ind,peak}}$ denote the respective peak flux densities; and $k$, $\alpha$, and $\beta$ are the Steinmetz parameters of the employed ferrite (N87 by EPCOS): $k = 14$, $\alpha = 1.72$, $\beta = 2.74$]. A core temperature of $T_{\text{core}} = 25°\text{C}$ is considered in order to account for increased core losses during the start-up phase of the converter (at $T_{\text{core}} = 25°\text{C}$ the N87 ferrite generates higher losses than at $T_{\text{core}} = 100°\text{C}$).

## IV. Weight Optimization of the DAB Converter

The HF transformer and inductor and the heat sink offer the greatest potential regarding a weight minimization of the complete DAB converter, and are therefore discussed in the subsequent Sections IV-A and IV-B. Section IV-C summarizes the converter design based on the evaluation of a $\gamma$-$\eta$-Pareto Front.

### A. Minimum Weight Transformer and Inductor

Fig. 10 depicts the general (scalable) setup of the HF transformer and the inductor: the LV winding encloses $n_{\text{tr,core}}$ ferrite E-cores (material: N87); the MV winding is placed around the LV winding (to simplify the isolation of the transformer's MV terminal) and encloses $n_{\text{tr,core}} + n_{\text{ind,core}}$ cores. The additional $n_{\text{ind,core}}$ E-cores form the inductor, where the required air gap, with the air gap length $l_{\text{air}}$, is located in the center core leg in order to achieve low HF losses in the MV winding. The copper foils and the heat pipes shown in Fig. 10 are used to extract the heat generated in the windings and the cores. The extracted heat is transported to a heat sink, which is mounted to the top of the transformer.

The employed optimization method calculates the losses and the weights of a large number of different transformer designs. The optimization procedure is detailed in [5]. It employs the parameters listed in Tab. III and yields the transformer and inductor design results given below.

- Transformer core: 2 stacked E42/21/20 core sets
- Inductor core: one E42/21/20 core set
- Number of turns: $N_1 = 21$, $N_2 = 28$
- Employed litz wire, LV side: $151 \times 0.071\,\text{mm}$
- Employed litz wire, MV side: $132 \times 0.071\,\text{mm}$
- Inductor air gap length:[4] $l_{\text{air}} = 3.3\,\text{mm}$
- Maximum copper losses, LV side: 17 W, MV side: 24 W
- Maximum core losses, transf.: 29 W, ind.: 8 W.

The DAB transformer is realized (Fig. 11) in order to verify the calculated weight, losses, and winding temperatures. The measured weight of the transformer is 510 g, which is 6% higher than the calculated weight (481 g). This difference is attributed to the gap filler used to reduce the thermal resistance between the litz wire and the teflon insulation.

[4]The given air gap length includes the increase of the effective core cross sectional area due to fringing fields at the air gap according to [12].

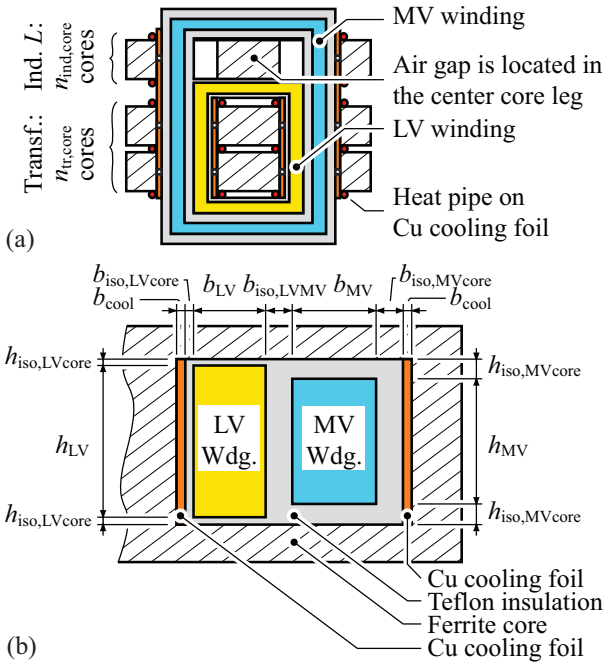


Fig. 10. Setup of the HF transformer and inductor; (a) top view; (b) cross sectional view of the winding window.

TABLE III

Parameters used to design the transformer.

| Property | Value | Description |
|---|---|---|
| $b_{\text{iso,LVcore}}$ | 0.2 mm | Insulation width between LV wdg. and core |
| $b_{\text{iso,LVMV}}$ | 2 mm | Insulation width between LV and MV wdgs. |
| $b_{\text{iso,MVcore}}$ | 2 mm | Insulation width between MV wdg. and core |
| $b_{\text{cool}}$ | 0.3 mm | Thickness of the copper foil used for cooling |
| $h_{\text{iso,LVcore}}$ | 0.2 mm | Insulation height between LV wdg. and core |
| $h_{\text{iso,MVcore}}$ | 2 mm | Insulation height between MV wdg. and core |
| $d_{\text{heat pipe}}$ | 3.0 mm | Diameter of the heat pipe |

The impedance measurement of the realized DAB transformer, with the LV side windings being shorted, reveals a MV side referred stray inductance of $L = 109\,\mu\text{H}$ (Fig. 12). However, an increased air gap length of $l_{\text{air}} = 4.2\,\text{mm}$ is required, since the stray inductance of the proposed setup, depicted in Fig. 10(a), is higher than calculated, which is mainly addressed to an increased stray field of the inductor part and needs to be investigated further. The measured magnetizing inductance is $L_{\text{M}} = 3.62\,\text{mH}$ and the resonance frequency (with the LV side being shorted) is 4.2 MHz, well above the switching frequency.

The total measured winding resistances,

$$R_{\text{tr,ind}}(f) = \frac{R_{\text{tr,LV}}(f)}{n^2} + R_{\text{tr,ind,MV}}(f), \tag{6}$$

are $R_{\text{tr,ind}}(f = 1\,\text{kHz}) = 372\,\text{m}\Omega$ at low frequencies and

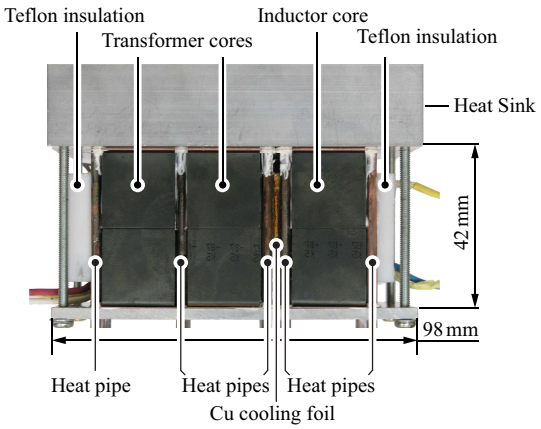


Fig. 11. Picture of the realized HF transformer and the inductor.

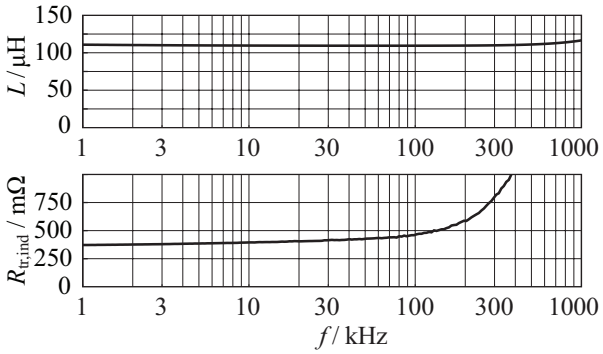


Fig. 12. Measured series inductance ($L$) and series resistance ($R_{\text{tr,ind}}$) of the HF transformer and inductor. The impedance is measured from the MV side with the LV side terminals being shorted. Employed impedance analyzer: Agilent 4294A Precision Impedance Analyzer; due to a impedance phase angle close to 90° the relative measurement error of the resistance measurement is large (±11% at $f = 100\,\text{kHz}$). The increase of $L$ starting at about 1 MHz is caused by the self resonance at 4.2 MHz.

$R_{\text{tr,ind}}(f = 100\,\text{kHz}) = 467\,\text{m}\Omega$ at the switching frequency (Fig. 12; measured at a temperature of 25°C). At low frequencies the calculated and the measured dc resistances fit well (calculated: $R_{\text{tr,ind}}(f \to 0) = 370\,\text{m}\Omega$). However, at $f = 100\,\text{kHz}$, the calculated ac resistance is considerably lower, $R_{\text{tr,ind}}(f = 100\,\text{kHz}) = 385\,\text{m}\Omega$. Further measurements show that the additional ac losses are generated in the copper foils, which are used to cool the transformer (cf. Fig. 10). It is therefore difficult to avoid these additional losses ($\approx 10\,\text{W}$ at $V_1 = V_{1,\text{min}}$ and $V_{2,i} = V_{2,i,\text{min}}$). However, the proposed transformer setup directly conducts these losses to a heat sink (via the heat pipes).

In order to verify the winding temperatures and the effectiveness of the cooling system, the transformer is assembled on an oversized heat sink with $R_{\text{th}} \approx 0.15\,\text{K/W}$, using forced air cooling. According to FEM simulations the proposed setup enables the core losses to be extracted much more effectively than the winding losses, i.e. the impact of the core losses on the winding temperature is small. Therefore, in a first step, only the impact of the winding losses on the winding temperature is measured. The measurement employs dc winding currents, which are equal to the ac currents given in Tab. I being multiplied with $\sqrt{R_{\text{tr,ind}}(f = 100\,\text{kHz})/R_{\text{tr,ind}}(f = 1\,\text{kHz})} = 1.1$, in order to generate the expected ac copper losses (LV side: 13.5 A, MV side: 10.1 A). The measured temperatures are 59°C and 67°C in the LV and MV side windings, respectively (heat sink temperature: 31°C). These results are considerably less than the calculated temperatures (78°C and 90°C in the LV winding and the MV winding, respectively), which is mainly due to the gap filler used to reduce the thermal resistance.

### B. Weight-Optimized Heat Sink Design Procedure

The results obtained in Section III and IV-A facilitate the calculation of the total losses of the full bridge, $P_{\text{loss,FB}}$, the NPC converter, $P_{\text{loss,NPC}}$, and the maximum total losses of the HF transformer and inductor, $P_{\text{loss,tr,ind}}$:[5]

$$P_{\text{loss,FB}} = 57\,\text{W},\ P_{\text{loss,NPC}} = 50\,\text{W},\ P_{\text{loss,tr,ind}} = 70\,\text{W} + 10\,\text{W}.$$

This enables the calculation of the respective heat sinks' thermal resistances,

$$R_{\text{th,FB}} = \frac{T_{\text{baseplate,FB}} - T_{\text{amb}}}{P_{\text{loss,FB}}},\ R_{\text{th,NPC}} = \frac{T_{\text{baseplate,NPC}} - T_{\text{amb}}}{P_{\text{loss,NPC}}},$$

$$R_{\text{th,tr,ind}} = \frac{T_{\text{baseplate,tr,ind}} - T_{\text{amb}}}{P_{\text{loss,tr,ind}}}, \tag{7}$$

($T_{\text{amb}} = 45°\text{C}$, $T_{\text{baseplate,FB}} = 110°\text{C}$, $T_{\text{baseplate,NPC}} = 110°\text{C}$, $T_{\text{baseplate,tr,ind}} = 85°\text{C}$), which subsequently facilitates the design of the related weight optimized heat sinks. The used heat sink optimization procedure is based on the method detailed in [13], which is modified in order to allow for an optimization with respect to minimum weight. Fig. 13 defines the geometric heat sink parameters and Tab. IV lists the calculated heat sinks.

TABLE IV

WEIGHT OPTIMIZED HEAT SINKS; ALL HEAT SINKS USE $b = 40\,\text{mm}$, $h = 40\,\text{mm}$, AND $d = 3\,\text{mm}$, CF. FIG. 13; EACH HEAT SINK EMPLOYS A SAN ACE 40 FAN (LV AND MV CONVERTERS: 109P0412S701, $m = 32\,\text{g}$; TRANSFORMER AND INDUCTOR: 109P0412K3013, $m = 52\,\text{g}$).

| | $l$ | $t$ | $n_{\text{ch}}$ | $R_{\text{th}}$ | $m$ |
|---|---|---|---|---|---|
| LV side full bridge | 47 mm | 1.1 mm | 9 | 1.1 K/W | 70 g |
| MV side NPC conv. | 47 mm | 1.1 mm | 8 | 1.25 K/W | 66 g |
| Transformer and ind. | 80 mm | 1.1 mm | 10 | 0.46 K/W | 128 g |

[5]For the operating point with the maximum copper losses of the transformer (minimum port voltages), the transformer core losses are minimum and for maximum core losses of the transformer the copper losses are minimum. Furthermore, additional eddy current losses in the cooling copper foils of approximately 10 W are included, cf. Section IV-A.

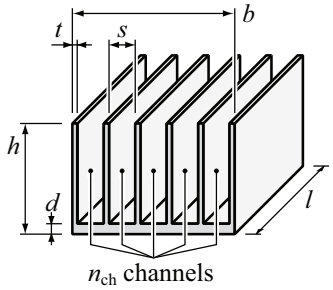


Fig. 13. Geometric heat sink parameters used in Tab. IV.

TABLE V
WEIGHT OF A SINGLE DAB CONVERTER MODULE (RATED OUTPUT POWER: 6.25 kW.

| Property | Value | Description |
|---|---|---|
| $m_{\text{LV,semi}}$ | 24 g | Semiconductor mass, LV side |
| $m_{\text{LV,driver}}$ | 80 g | Mass of the gate drivers, LV side |
| $m_{\text{LV,PCB}}$ | 40 g | Estimated mass of the PCB, LV side |
| $m_{C1}$ | 65 g | Estimated mass of $C_1$ |
| $m_{Cd}$ | 15 g | Estimated mass of the decoupling capacitor $C_d$ |
| $m_{\text{LV,hs}}+m_{\text{fan}}$ | 102 g | Heat sink and fan of the LV side |
| $m_{\text{MV,semi}}$ | 30 g | Semiconductor mass, MV side |
| $m_{\text{MV,driver}}$ | 80 g | Mass of the gate drivers, MV side |
| $m_{\text{MV,PCB}}$ | 50 g | Estimated mass of the PCB, MV side |
| $m_{C2a}+m_{C2b}$ | 130 g | Sum of the estimated mass of $C_{2a}$ and $C_{2b}$ |
| $m_{\text{MV,hs}}+m_{\text{fan}}$ | 98 g | Heat sink and fan of the MV side |
| $m_{\text{tr}}+m_{\text{ind}}$ | 481 g | Mass of the transformer and the inductor |
| $m_{\text{tr,ind,hs}}+$ | 235 g | Transformer and inductor heat sink |
| $m_{\text{fan}}$ | | (includes 14 heat pipes, 2nd base plate and fan) |
| $m_{\text{DAB}}$ | 1430 g | Estimated mass of a single DAB module |

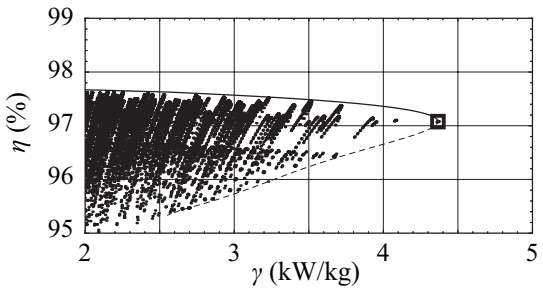


Fig. 14. $\gamma$-$\eta$-Pareto Front for the DAB converter; the □ symbol denotes the selected design.

### C. Minimum Weight DAB Converter

Based on the presented design procedures all converter components can be determined [5]. Tab. V summarizes the components' and heat sinks' weights.

Fig. 14 depicts the resulting power-to-weight ratio $\gamma$ and the efficiency $\eta$ of the DAB converter,

$$\gamma = \frac{P_{\text{out}}}{m_{\text{DAB}}} \quad \text{and} \quad \eta = \frac{P_{\text{out}}}{P_{\text{in}}}, \tag{8}$$

calculated for the different HF transformer and inductor designs obtained from the procedure detailed in [5]. The maximum achievable power-to-weight ratio is $\gamma = 4.4\,\text{kW/kg}$ at $\eta = 97\%$ (assuming nominal operation with $V_1 = 700\,\text{V}$ and including an auxiliary power demand of $P_{\text{aux}} = 27\,\text{W}$ for the fans, the gate drivers, and the control board).

## V. CONCLUSIONS

The method used to design a minimum weight bidirectional DAB dc–dc converter with a rated power of $6.25\,\text{kW}$ is presented in this paper. The DAB converter is used to provide a dc voltage of $8\,\text{kV}$ to the tether of an AWT generator system with a rated power of $100\,\text{kW}$. The employed design method results in a $\gamma$-$\eta$-Pareto Front. For the minimum weight DAB converter a power-to-weight ratio of $\gamma = 4.4\,\text{kW/kg}$ and an efficiency of $\eta = 97\%$ are calculated. The HF transformer and inductor are realized in order to verify the calculated weight, losses, and temperature inside the transformer windings. With the obtained results the realization of the DAB dc–dc converter is directly feasible.

The presented results clearly identify light weight / low volume medium voltage converter systems as suitable application for the SiC JFET, which are characterized by low on-state resistance at a high blocking voltage and low switching losses.

## REFERENCES

[1] M. L. Loyd, "Crosswind kite power," *Journal of Energy*, vol. 4, no. 3, pp. 106–111, May/June 1980.
[2] Joby Energy. Accessed: April 2011. [Online]. Available: http://www.jobyenergy.com.
[3] Makani Power. Accessed: April 2011. [Online]. Available: http://www.makanipower.com
[4] Sky WindPower. Accessed: April 2011. [Online]. Available: http://www.skywindpower.com
[5] J. W. Kolar, T. Friedli, F. Krismer, A. Looser, M. Schweizer, P. Steimer, J. Bevirt, "Conceptualization and multi-objective optimization of the electric system of Airborne Wind Turbines" in *Proc. IEEE 2011 International Symposium on Industrial Electronics (ISIE'11)*, June 2011, pp. 32–55.
[6] C. Arrioja, S. Kenzelmann, A. Rufer, "Reversible DC/DC converter as interface between low and medium voltage DC networks", in *Proc. 31st European Power Electronics / Intelligent Motion / Power Quality Conference (PCIM'11)*, Nuremberg, Germany, May 17–19, 2011, pp. 253–258.
[7] D. Aggeler, J. Biela and J. W. Kolar, "Controllable dv/dt-behaviour of the SiC MOSFET/JFET cascode an alternative hard commutated switch for telecom applications," in *Proc. IEEE 25th Applied Power Electronics Conference and Exposition (APEC'10)*, Palm Springs, USA, Feb. 21–25, 2010, pp. 1584–1590.
[8] F. Krismer and J. W. Kolar, "Closed form solution for minimum conduction loss modulation of DAB converters," *IEEE Trans. Power Electron.*, vol. PP, pp. 1–16, May 2011, acepted for future publication.
[9] M. H. Kheraluwala, R. W. Gascoigne, D. M. Divan, and E. D. Baumann, "Performance characterization of a high-power dual active bridge dc-to-dc converter," *IEEE Trans. Ind. Appl.*, vol. 28, no. 6, pp. 1294–1301, Nov./Dec. 1992.
[10] F. Krismer and J. W. Kolar, "Accurate power loss model derivation of a high-current dual active bridge converter for an automotive application," *IEEE Trans. Ind. Electron.*, vol. 57, no. 3, pp. 881–891, Mar. 2010.
[11] F. Krismer, "Modeling and optimization of bidirectional dual active bridge dc–dc converter topologies," Ph.D. dissertation, Swiss Federal Institute of Technology Zurich (ETH Zurich), 2010.
[12] A. van den Bossche and V. C. Valchev, *Inductors and transformers for power electronics.* New York, NY: Taylor & Francis, 2005.
[13] U. Drofenik, G. Laimer, and J. W. Kolar, "Theoretical converter power density limits for forced convection cooling," in *Proc. 26th European Power Electronics / Intelligent Motion / Power Quality Conference (PCIM'05)*, Nuremberg, Germany, June 7–9, 2005, pp. 1–12.